

See discussions, stats, and author profiles for this publication at: <https://www.researchgate.net/publication/320309266>

Tree-Inspired Design for High-Efficiency Water Extraction

Article in *Advanced Materials* · October 2017

DOI: 10.1002/adma.201704107

CITATIONS

0

READS

123

18 authors, including:



Yiju Li

Harbin Engineering University

47 PUBLICATIONS 427 CITATIONS

SEE PROFILE



Feng Jiang

University of California, Davis

41 PUBLICATIONS 531 CITATIONS

SEE PROFILE



Jiayu Wan

University of Maryland, College Park

47 PUBLICATIONS 1,180 CITATIONS

SEE PROFILE



Siddhartha Das

University of Maryland, College Park

110 PUBLICATIONS 1,228 CITATIONS

SEE PROFILE

Some of the authors of this publication are also working on these related projects:



Oil-water interfacial mechanics [View project](#)



Nanocellulose [View project](#)

All content following this page was uploaded by [Chao Jia](#) on 13 October 2017.

The user has requested enhancement of the downloaded file.

Tree-Inspired Design for High-Efficiency Water Extraction

Mingwei Zhu, Yiju Li, Guang Chen, Feng Jiang, Zhi Yang, Xiaoguang Luo, Yanbin Wang, Steven D. Lacey, Jiaqi Dai, Chengwei Wang, Chao Jia, Jiayu Wan, Yonggang Yao, Amy Gong, Bao Yang, Zongfu Yu, Siddhartha Das,* and Liangbing Hu*

The solar steam process, akin to the natural water cycle, is considered to be an attractive approach to address water scarcity issues globally. However, water extraction from groundwater, for example, has not been demonstrated using these existing technologies. Additionally, there are major unaddressed challenges in extracting potable water from seawater including salt accumulation and long-term evaporation stability, which warrant further investigation. Herein, a high-performance solar steam device composed entirely of natural wood is reported. The pristine, natural wood is cut along the transverse direction and the top surface is carbonized to create a unique bilayer structure. This tree-inspired design offers distinct advantages for water extraction, including rapid water transport and evaporation in the mesoporous wood, high light absorption ($\approx 99\%$) within the surface carbonized open wood channels, a low thermal conductivity to avoid thermal loss, and cost effectiveness. The device also exhibits long-term stability in seawater without salt accumulation as well as high performance for underground water extraction. The tree-inspired design offers an inexpensive and scalable solar energy harvesting and steam generation technology that can provide clean water globally, especially for rural or remote areas where water is not only scarce but also limited by water extraction materials and methods.


Water shortage is one of the most pressing global challenges. Solar-driven water desalination is particularly attractive due to the abundance of solar energy as well as its negligible environmental impacts.^[1–5] Recently, the use of new materials such as graphene, gold nanoparticles, and amorphous carbon has

advanced the field of solar-driven water desalination.^[4–12] However, there are still tremendous challenges that need to be addressed including material cost as well as mitigating device performance degradation. For example, plasmonic metal nanoparticles are expensive and corrode in water, which limits the lifetime of the desalination device. Therefore, research efforts related to the design of solar steam generation devices composed of inexpensive and naturally abundant materials have recently flourished: the fabrication of a carbon foam/exfoliated graphene bilayer structure,^[6] a trilayer structure composed of transparent bubble wrap/commercial cermet/polystyrene foam,^[1] a carbonized mushroom/polystyrene foam,^[13] a graphene oxide-based aerogel,^[14] and a graphene oxide-coated wood.^[15] To date, the majority of these novel solar steam technologies were demonstrated using deionized water and thus salt accumulation (including both the precipitation of soluble salts beyond the saturation concentration and the formation of sparingly soluble salts) was not considered. Only a few studies utilized seawater; however, salt accumulation issues were not addressed in detail.^[3,15,16] In fact, salt accumulation often occurs with practical thermal desalination systems and should merit serious consideration in terms of salt removal methods.^[17] It is expected that to effectively reduce the salt blockage during the steam extraction process from seawater, large microsized channels throughout the material are required to facilitate device regeneration. In this way, the accumulated salts can dissolve (i.e., water soluble salts such as NaCl and KCl) and/or fall back to the surrounding seawater (i.e., sparingly soluble salts such as calcium carbonate, calcium sulfate, and magnesium hydroxide) at night. Note that all previous works extract fresh water directly from water sources. Extracting potable water from the ground (sand or soil) is of critical importance in arid environments where sufficient water sources are lacking; however, no investigations have been conducted to date.^[18–20] Therefore, a solar steam device that can simultaneously address all the aforementioned issues, including the use of low cost materials and inexpensive fabrication methods, facile device regeneration to circumvent salt accumulation, and structural integrity of the groundwater extraction device, is vital to the advancement of the solar steam

Prof. M. Zhu, Y. Li, Dr. F. Jiang, S. D. Lacey, J. Dai, Dr. C. Wang, C. Jia, Dr. J. Wan, Y. Yao, Dr. A. Gong, Prof. L. Hu
Department of Materials Science and Engineering
University of Maryland
College Park, MD 20742, USA
E-mail: binghu@umd.edu

Dr. G. Chen, Z. Yang, Y. Wang, Prof. B. Yang, Prof. S. Das
Department of Mechanical Engineering
University of Maryland
College Park, MD 20742, USA
E-mail: sidd@umd.edu

X. Luo, Prof. Z. Yu
Electrical and Computer Engineering
University of Wisconsin-Madison
Madison, WI 53706, USA

 The ORCID identification number(s) for the author(s) of this article can be found under <https://doi.org/10.1002/adma.201704107>.

DOI: 10.1002/adma.201704107

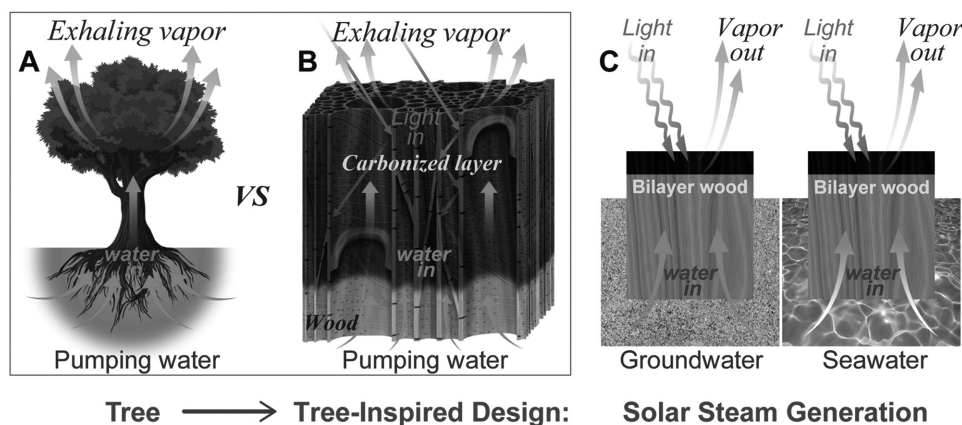


Figure 1. Schematic demonstrating the working principle of bilayer wood as an inexpensive, scalable, and efficient solar-driven water desalination material. A) Schematic of a tree pumping water from the ground to the treetop to sustain photosynthesis. B) Illustration of the tree-inspired design using a bilayer wood structure. The top carbonized portion acts as an efficient 3D light absorber layer while the pristine wood portion is hydrophilic, which promotes rapid water transport for continuous solar steam operation. Note that the wood is cut perpendicular to the growth direction so that the natural wood channels are preserved. C) Water extraction capabilities of the bilayer wood with different media: groundwater (from sand or soil) and seawater. The bilayer structure provides an efficient means of steam generation by solar-driven desalination.

field. Note that efficient solar steam-based water extraction devices should also share the same attributes as other reported devices: rapid water transport, high solar absorption, efficient solar steam evaporation, and excellent thermal isolation.^[3,6,21]

Trees are the most abundant biofactories on earth and play a critical function in the ecosystem by sustaining human, animal, and plant life. A living tree is constantly circulating water from the ground upstream (transpiration) by relying on the wood mesostructures.^[21] When transported to leaves, the water molecules will participate in the photosynthesis process producing glucose. Simultaneously, O_2 is produced and released for the respiration of living organisms. Herein, we propose a “tree-inspired design” using natural wood with a bilayer structure (Figure 1) for solar steam generation, including seawater desalination and groundwater extraction (from sand and soil). This wood-based device has interconnected channels (fiber tracheids and vessels with lumen diameters in the tens of micrometers) within the top “light absorbing” layer as well as the bottom “water pumping” layer. There is a perfect microstructural match at the interface between the carbonized wood and natural wood section, which facilitates efficient water extraction from the ground as well as the production of water vapor under solar illumination. Additionally, the microsized through-channels dramatically reduce salt accumulation during device operation due to highly efficient mass exchange with the seawater source. Note that the wood device can also be implanted into the ground for the extraction of water from soil and sand.

The proposed bilayer wood structure is easily fabricated in two steps: (1) cut the wood perpendicular to the wood growth direction and (2) carbonize the wood surface by heating for 0.5 min at 500 °C. In our work, a common hardwood, American basswood, was chosen due to its abundance, low cost, and naturally aligned wood channels. By carbonizing the top surface in a controlled manner, a seamless bilayer structure is achieved and the overall microstructure of the wood can be retained. Note that the typical thickness of the carbonized layer and the pristine natural wood layer in the proposed device are 3 mm and 3 cm, respectively. After carbonization, the (top) carbonized

layer can absorb sunlight more effectively than the natural wood layer while the (bottom) natural wood layer provides an avenue for rapid and efficient water transport, which is essential for continuous device operation. Additionally, the low thermal conductivity of the natural wood layer drastically reduces the heat dissipation from the top carbonized surface. Consequently, the all-wood solar desalination device can meet the requirements for large-scale production due to the use of both inexpensive, readily available materials as well as facile fabrication methods.

In trees, the mesoporous wood channels help to pump water upward through a process known as transpiration (Figure 1A). In our tree-inspired design, the carbonized surface layer efficiently absorbs the solar illumination causing the temperature of the bilayer wood to increase and evaporation to occur at the top surface (Figure 1B). In this way, the proposed bilayer wood design can efficiently extract water when the device is placed in the ground (sand or soil) or in seawater, as shown schematically in Figure 1C. A continuous flow of water is maintained due to the absorptive nature of the hydrophilic polysaccharides (cellulose microfibrils and hemicellulose) embedded within the lignocellulosic walls. The inherent mesoporous wood structure also induces a capillary effect due to the fiber tracheids and vessels. Notably, the open microchannels within the carbonized top layer allow water vapor/steam to escape without interference from any crystallized salt that may build up during the evaporation process. Since the natural wood has a low thermal conductivity ($\approx 0.2 \text{ W m}^{-1} \text{ K}^{-1}$), the absorbed heat from the illuminated carbonized surface layer can be concentrated and efficiently used. The performance of the all-wood solar-driven desalination device was tested without further modifications or processing steps. The bilayer wood structure achieved the following performance metrics in terms of solar-driven desalination: (1) $\approx 99\%$ light absorption; (2) 87% efficiency under 10 sun illumination; (3) linear operation up to 10 suns; (4) stable operation without corrosion or solar degradation (under 5 sun illumination for 100 h); (5) long-term stability in seawater without salt accumulation, and (6) successful water extraction directly from the ground (sand and soil).

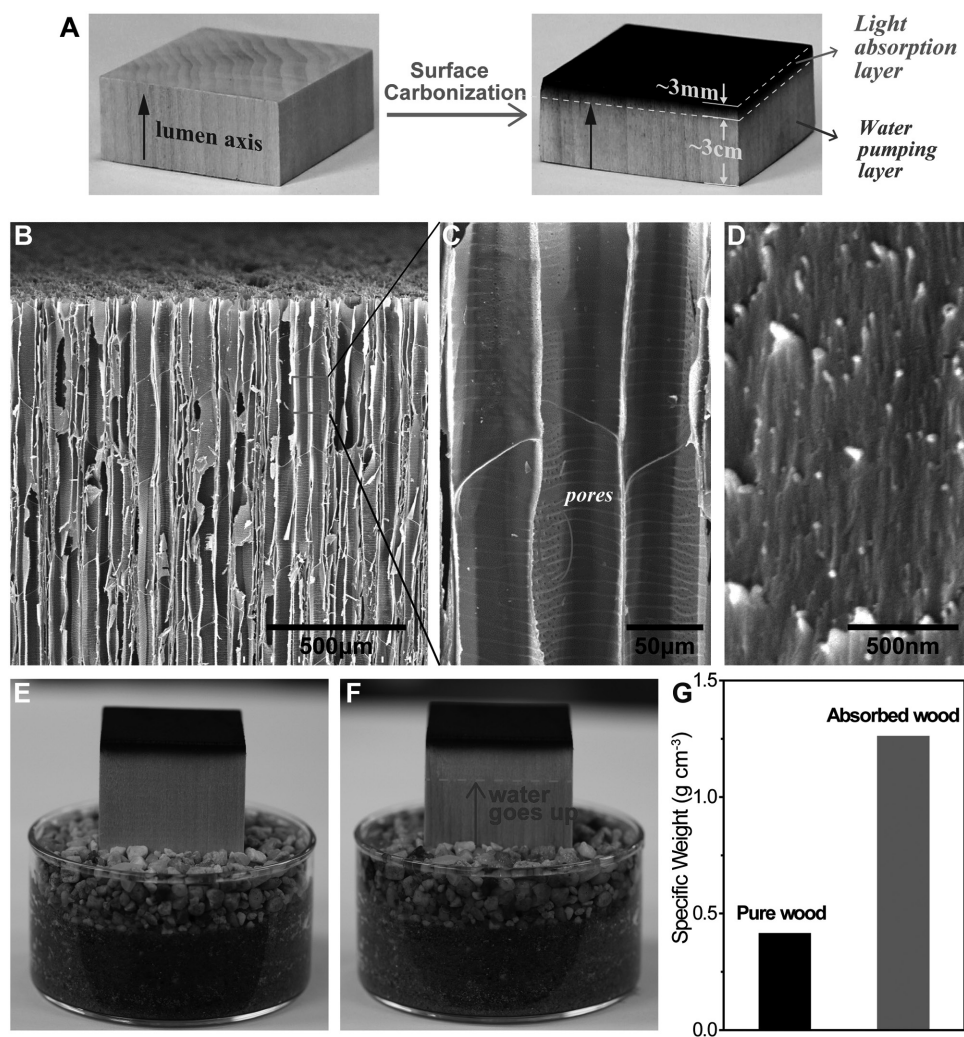


Figure 2. Characterization, fabrication, and feasibility of bilayer wood as a water extraction material. A) The facile fabrication process used to create bilayer wood: (1) wood is cut perpendicular to the lumen axis to the desired height (typically several centimeters) and (2) a controllable surface carbonization process is employed to form a thin layer (≈ 3 mm) of amorphous carbon. Note that the carbonized wood surface acts as an efficient light absorption layer. B) SEM image of the long, aligned wood microchannels (fiber tracheids and vessel lumens) within the bilayer wood that facilitate the transport of both water and steam/vapor. C) Higher magnification SEM image of the vessel lumens, which consist of small pits that decorate the inner surface of the wood channels. These pits facilitate water transport to the neighboring lumen. D) SEM image showing a detailed view of the cell wall, where aligned cellulose microfibrils are embedded within the lignocellulosic matrices. E,F) Experimental demonstration of water absorption within the bilayer wood device. G) The specific weight of bilayer wood ($4.5\text{ cm} \times 4.5\text{ cm} \times 2.9\text{ cm}$) before and after saturation with the absorbed water.

Unlike conventional solar steam extraction materials, the layers of the bilayer wood are seamlessly integrated to ensure long-term stability without interface degradation. Digital images of the basswood before and after surface carbonization are shown in **Figure 2A** and **Figure S1** (Supporting Information), where the specific wood layers (carbonized layer and natural wood layer) promote enhanced solar absorption and water transport, respectively. The microstructure of the bilayer wood device was elucidated using scanning electron microscopy (SEM). The hardwood cells are primarily composed of fiber tracheids and vessels with lumen diameters ranging from 10–100 μm (**Figure 2B,C**; **Figures S2** and **S3**, Supporting Information), which act as highways for rapid water transport.^[22,23] In the wood cell walls, cellulose microfibrils (**Figure 2D**) are embedded within the lignocellulosic matrices. Previous

studies have shown that these fibrils can be extracted and served as the main building blocks to fabricate various hierarchical structures.^[24–29] The lignin reinforces the cell walls to improve the wood's mechanical properties as well as reduce the permeability of water. In this way, the water can be confined to the vascular lumens; however, lateral water transport is still possible through the pits, which also reduces the risk of cavitation-induced embolism.^[30,31] After the surface carbonization treatment, the microscopic wood structures are well preserved (**Figure 2B**; **Figures S4–S6**, Supporting Information). As expected, the natural wood provides excellent water absorption due to synergistic effects between the vascular lumens and absorptive cellulose microfibrils (**Figure 2E, F**). The capillary effects induced by the surface tension of water also ensure that the water level within the microchannels reaches 35.2 cm,

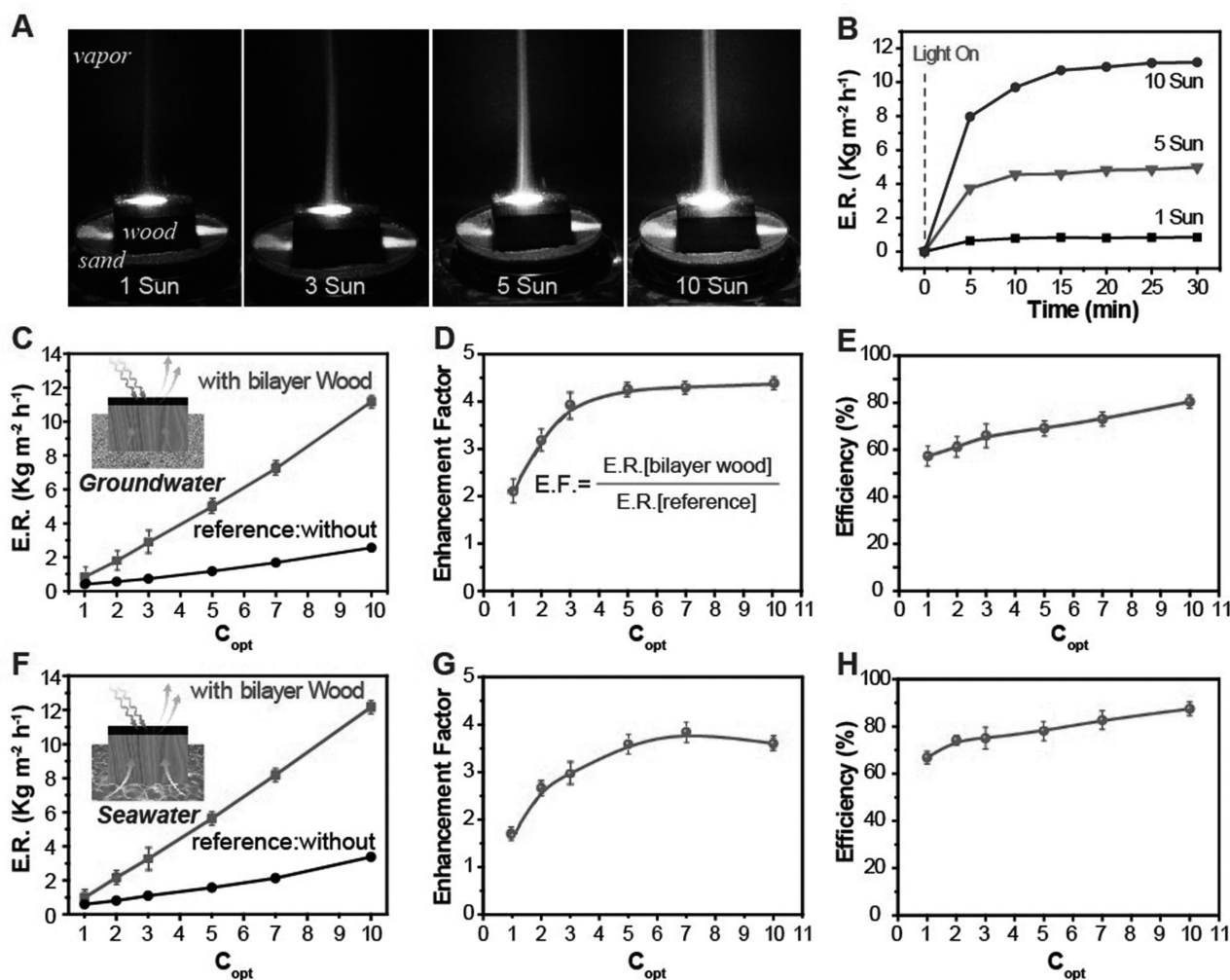


Figure 3. Solar steam generation performance of bilayer wood from groundwater (wet sand) and seawater. A) Digital images of steam coming from the bilayer wood surface at various light intensities: 1, 3, 5, and 10 suns. B) The dynamics of solar steam generation at different light intensities. Within 15 min, the evaporation rates reach nearly the maximum value under each solar concentration. C) Groundwater extraction performance of the bilayer wood placed in wet sand. The water evaporation rate and the intensity of the incident illumination are denoted as E.R. and C_{opt} , respectively. Note that the control experiment (without bilayer wood) was carried out using identical environments (i.e., wet sand) at the same solar illumination intensity, where $1 C_{opt} = 1 \text{ kW m}^{-2}$. D) The E.F. of the bilayer wood for the groundwater experiments. As the light intensity increases, the bilayer wood exhibits enhanced solar steam generation. E.F. refers to the evaporation rate ratio with and without bilayer wood under different illumination intensities. E) Solar steam generation efficiency at different light intensities using bilayer wood for groundwater extraction. F) Desalinated water extraction performance of the bilayer wood placed in seawater. Note that the control experiment (without bilayer wood) was carried out using seawater subjected to the same illumination intensity and experimental conditions. G) The E.F. of the bilayer wood at different light intensities for the seawater experiments. H) Solar steam generation efficiency at different light intensities for the bilayer wood device in seawater.

which is much larger than the overall device thickness (Static Height Calculation; Table S1 and Figure S7, Supporting Information). After spontaneous water absorption, the density of the bilayer wood increases from 0.41 to 1.26 g cm^{-3} (Figure 2G).

The bilayer wood extracts water efficiently under solar illumination. When the bilayer wood is placed in sand or soil, groundwater can be readily extracted due to the capillary effect that occurs within the wood mesostructures. This is a unique water transport/extraction ability that has only been demonstrated with the proposed bilayer wood structure due to the following factors: basswood possesses long, open micro-sized channels and exhibits suitable mechanical properties. Figure 3A and Figure S8 (Supporting Information) display the experimental

setup for steam generation. Note that factors such as temperature, humidity, and wind speed could adversely affect the evaporation rate of an open system during testing. To avoid these potential issues, a constant room temperature and humidity level were maintained in the lab environment. A glass housing also protected the device during testing. First, the bilayer wood was placed into a dish filled with wet sand while a balance monitored the weight loss over time. A solar simulator exposed the top carbonized wood surface to various illumination intensities (1–10 suns). Figure 3A shows the column of steam that expands as the illumination intensity increases, indicative of faster evaporation rates. Under solar illumination, solar steam is stably generated when the bilayer wood was inserted directly

into the wet sand. To mimic an arid environment, the wet sand was covered with a layer of dry sand before testing under the aforementioned conditions. Note that the evaporation rates measured during the dark condition (no light exposure) were subtracted out from each evaporation rate reported in this work (Figure S9, Supporting Information). The evaporation rates (E.R.s) versus time for various illumination intensities are shown in Figure 3B. The E.R. attains a maximum value within minutes, which indicates a continuous water supply is readily achieved when the bilayer wood is exposed to solar illumination. Under 10 suns, the E.R. for the generated solar steam exceeded $11.2 \text{ kg m}^{-2} \text{ h}^{-1}$. The E.R. versus optical concentration (C_{opt}) is shown in Figure 3C. Under an identical illumination intensity, the steam generated with the proposed bilayer wood structure drastically exceeds the performance of pure sand. To illustrate this difference, an enhancement factor (E.F.) was calculated and plotted against the optical concentration (Figure 3D). The E.F. takes into account the water E.R. of the wet sand for both test conditions: with and without the bilayer wood. Notably, this is the first time a solar steam method has successfully extracted groundwater. The corresponding solar steam generation efficiency η (Figure 3E) of the bilayer wood can be calculated using the following equation^[1,4,6,8,11,13]

$$\eta = \dot{m} h_{\text{LV}} / C_{\text{opt}} P_0 \quad (1)$$

where \dot{m} ($\text{kg m}^{-2} \text{ h}^{-1}$) denotes the evaporation rate, C_{opt} is the optical concentration, and h_{LV} is the total enthalpy of the liquid–vapor phase transition including the sensible heat. Note that P_0 represents the nominal solar irradiation value of 1 kW m^{-2} .

The thermal efficiency of the bilayer wood solar steam generator under various illumination levels is shown in Figure 3E. Note that the evaporation efficiency increases from 57.3% at 1 kW m^{-2} to 80.4% at 10 kW m^{-2} (Figure 3E). The water extraction performance of the bilayer wood was also tested in other media including sand and soil for groundwater extraction as well as seawater (Figure 3F). Control experiments with pure water under various illumination intensities were also carried out for comparison purposes. The performance of the bilayer wood in seawater is comparable to the recent work of Zhou et al., who used complex metal nanoparticles on expensive nanoporous anodic aluminum oxide membranes.^[3] Unlike Zhou et al., our natural bilayer wood design is scalable. The E.F. for seawater is shown in Figure 3G. Notably, the bilayer wood exhibited enhanced performance in seawater compared to the media for groundwater (Figure 3H). Under 10 suns, the E.R. for the solar steam generated exceeded $12.2 \text{ kg m}^{-2} \text{ h}^{-1}$ with an efficiency of $\approx 90\%$. The reason why the water evaporation rate of the bilayer wood in sand is slightly lower than seawater may be attributed to a sealing effect associated with the groundwater and sand during the evaporation experiments. When the bilayer wood is placed into the wet sand, the wood channels will be partially blocked by the sand, which leads to slower water transport rates within the wood block. As a result, the evaporation rates of the bilayer wood in sand are relatively lower than in seawater where water transport routes are likely unimpeded. It should also be noted that water retrieval is an important aspect of desalination technologies. The water retrieval method can affect the solar steam generation process and thus

the water retrieval efficiency (from vapor) is an essential performance metric. However, in this work, we mainly focus on the material and the device design for solar steam generation and do not emphasize water retrieval since it is out of the scope of this study. Based on our results, we expect the bilayer wood to demonstrate comparable water extraction performance when the water resides $\approx 35 \text{ cm}$ below ground level (Static Height Calculation, Supporting Information). This feat has not been demonstrated by other solar steam materials and is a unique feature of the reported tree-inspired design.

The efficient solar steam generation from the bilayer basswood arises from its unique hierarchical structure, which facilitates both light/thermal management and fluidic transport (Figure 4). As illustrated in Figure 4A and Figure S10 (Supporting Information), the top carbonized layer functions as a highly efficient light absorber. In this case, the carbonized channels can guide the incident light via numerous reflections throughout the wood mesostructures (vessels) to facilitate enhanced light absorption. In the full-wave optical absorption simulation, periodic arrays of square holes within the black carbon are used for modeling purposes (Optical Modeling in Wood with a Broad Distribution of Hole Sizes; Figure S11, Supporting Information). The following values were used: a wavelength of 550 nm and a dielectric constant for carbon of $\epsilon = 4.34 + 3.68i$.^[32] Additionally, the orientation of the pores was assumed to be at an incident angle of $\theta = 10^\circ$. The modeling results (Figure 4B) indicate that while the wood channels with a larger diameter (up to $50\text{--}100 \mu\text{m}$) can guide light deeper into the wood block, the surface of the smaller channels (diameter $\approx 10 \mu\text{m}$) predominantly absorb the incident light. The light absorption for the bilayer wood, natural wood, and amorphous carbon was experimentally measured (Figure 4C). The bilayer wood with a carbonized surface treatment exhibits a broadband light absorption approaching 99% over almost the entire measured wavelength range. Notably, the light absorption is much higher than the natural wood, especially in the visible range. While the carbonized layer enhances light absorption for solar steam generation, the bottom natural wood layer provides excellent thermal isolation and rapid water transport when inserted into the ground or seawater. To illustrate this, the temperature distribution of the bilayer wood under different illumination intensities was monitored with an infrared radiation (IR) camera (Figure 4D; Figure S12, Supporting Information). Stable surface temperatures of 28.3 , 34.7 , 42.3 , and $57.4 \text{ }^\circ\text{C}$, were measured at 1, 2, 3, and 5 suns, respectively. These results indicate that the bilayer wood can attain a high solar steam generation efficiency at relatively low surface temperatures. Note that the natural wood has a low thermal conductivity of $0.2 \text{ W m}^{-1} \text{ K}^{-1}$, which mitigates thermal dissipation from the top carbonized wood surface when exposed to solar illumination.

The wood microstructures provide unique water transport characteristics. As shown in the SEM image in Figure 4E, each vessel (with an average size $d_v \approx 50 \mu\text{m}$) of the basswood is surrounded by fiber tracheids (with an average size $d_t \approx 5\text{--}15 \mu\text{m}$). The cell walls of both the vessels and fiber tracheids are composed of cellulose microfibrils embedded within the lignocellulosic matrices. This ensures that the walls are nearly impenetrable and can confine the water transport within the

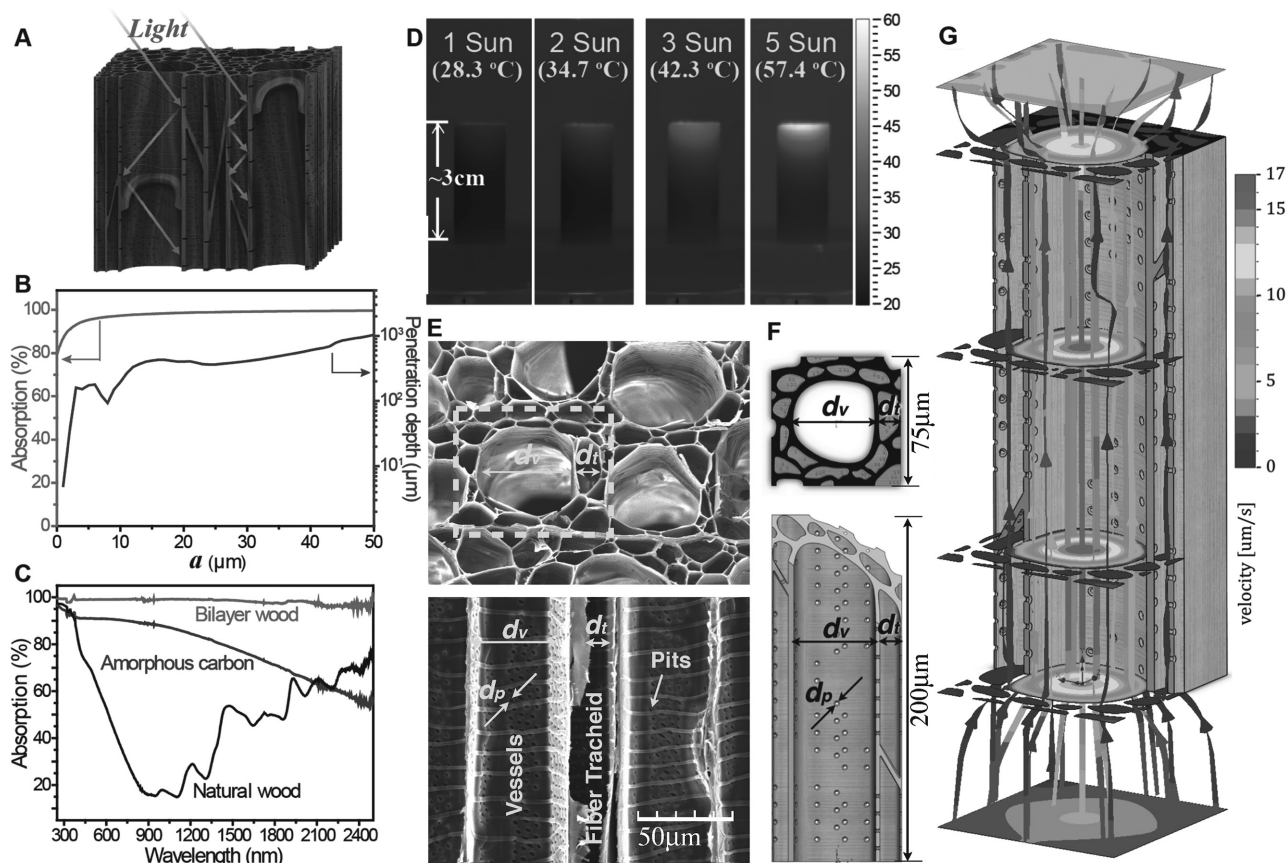


Figure 4. The unique advantages of bilayer wood for solar steam generation: light and thermal management as well as fluidic transport. A) Bilayer wood schematic demonstrating the light trapping, absorption, and thermal isolation capabilities due to the wood's unique microstructure. Each capability contributes to the high solar steam generation efficiency exhibited by the tree-inspired design. B) Simulation of how light interacts with the bilayer wood. The absorption and penetration depths with different hole sizes were explored. The wide hole size distribution leads to 3D light absorption within the wood structure. C) Experimentally measured light absorption spectra for bilayer wood, amorphous carbon, and natural wood. The bilayer wood absorbs nearly all the incident light over the entire wavelength range due to synergistic effects between the wood's microstructure and dual layer composition. D) IR images showing the temperature distribution of the bilayer wood at different illumination intensities. E) SEM image of the top carbonized surface where vessels are surrounded by tracheids (top image) as well as a cross-sectional view of the basswood microstructure comprised of vessels, fiber tracheids, and pits (bottom image). F) The 3D CAD model based on the structural parameters obtained from the SEM images shown in (E). G) Water velocity contours shown at various cross-sections along the wood channel. The water trajectories through the wood microstructure and velocity contours at various heights are color-coordinated based on the velocity magnitudes.

vascular lumens.^[30] However, the vessels and fiber tracheids remain connected via pits ($d_p \approx 2 \mu\text{m}$), which are located throughout the cell walls.^[31] A unique ability of the wood is the rapid transport of water through the structure when in contact with the water underneath. This water transport capability stems from the mesoporous and hydrophilic nature of the basswood (Figure 4E), computational fluid dynamics (CFD) simulations were conducted on one repeating block unit ($75 \times 75 \mu\text{m}^2$, as shown in Figure 4F; Figures S13 and S14, Supporting Information) using SOLIDWORKS. In the present study, the height of the wood block ($\approx 3 \text{ cm}$) is much smaller than the maximum height (35 cm) attainable by the capillary rise of water. Note that this maximum height is obtained by balancing the forces between surface tension and the weight of the rising water (i.e., the Jurin height; Static Height Calculation, Supporting Information).^[33,34] Consequently, a thin water film ($\approx 25 \mu\text{m}$) is apparent^[35] on the top wood surface ($\approx 3 \text{ cm}$ from the base

water surface) since the water evaporated (average evaporation rate of $3 \mu\text{m s}^{-1}$ under 10 suns) is continuously replenished by capillary-driven water ascension (filling rate of 5 mm s^{-1} at 3 cm above the water surface) (Calculation of the Filling Velocity; Figures S15 and S16, Supporting Information).

The derived water trajectories depicted in Figure 4G (CFD simulation) indicate that the vessels provide the dominant pathways for water to ascend the wood microstructure. The velocity contours at various heights show the water flux/transport through the open-ended vessels located in the middle of the wood structure. On the contrary, one witnesses a very low water flux inside the tracheids with smaller lumen size and intermittent closed ends. In this scenario, the tracheids act as obstacles that limit water transport, despite the fact that these structures are connected to the middle vessel via massive pits. The 3D CFD simulation also demonstrates that the pits have little involvement regarding water transport along the vessels. Consequently, the effective capillary size for evaporation-driven

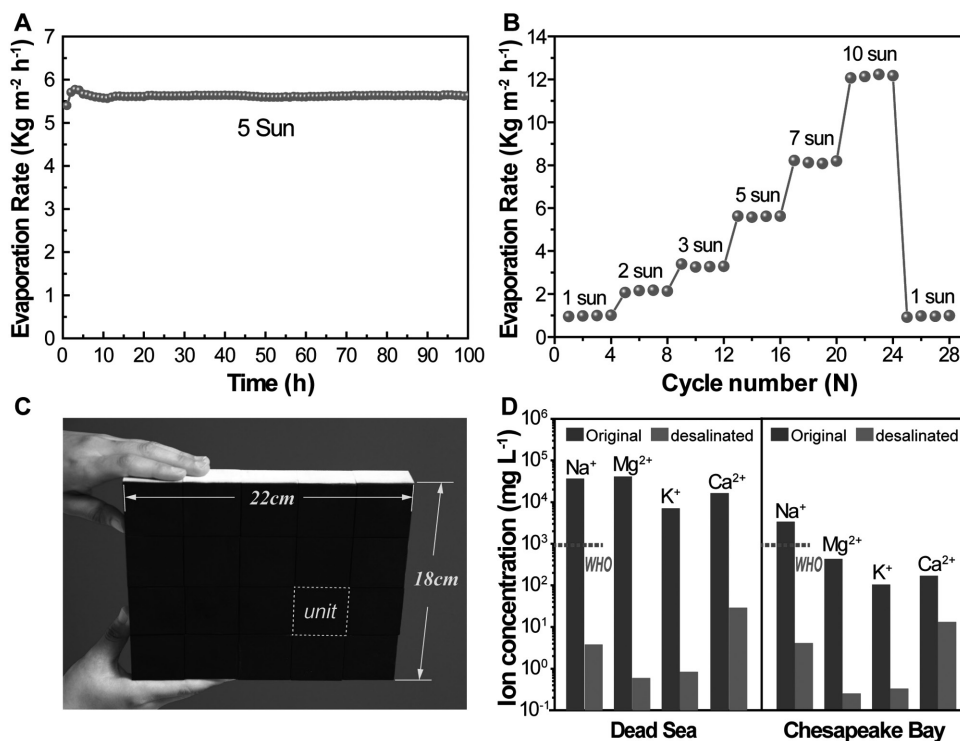


Figure 5. The stability, scalability, and desalination effects of bilayer wood for practical water extraction applications. A) The water evaporation stability (E.R. vs time) of the bilayer wood using Chesapeake Bay seawater. B) The measured evaporation cycle performance of the bilayer wood under different solar concentrations using Chesapeake Bay seawater. C) A 22 cm × 18 cm bilayer wood panel assembled with smaller bilayer wood blocks for scalable water extraction. D) The measured concentrations of four primary ions in the seawater samples (from the Chesapeake Bay in Maryland, with an average salinity of ≈1.05 wt%, and from the Dead Sea in Israel, with an average salinity of ≈27.69 wt%) before and after desalination with bilayer wood.

water transport through the basswood is predominantly determined by the lumen size of the open-ended vessels (see the Supporting Information for more discussion on flow physics).

The carbonized wood is stable in air, which is ideal to avoid material degradation under highly concentrated solar steam conditions. The two wood-based layers are seamlessly integrated, which avoids the typical degradation effects plaguing conventional water extraction and solar steam materials (e.g., oxidation, detachment, and agglomeration, especially with nanoparticles). The bilayer wood operates in a continuous and stable manner for 100 h under 5 suns in seawater (Figure 5A). Note that salt deposition is only apparent at illumination intensities ≥5 suns. This indicates that at higher illumination intensities, the surface evaporated water cannot be readily replenished by the water that refills the channels. In this case, the amount of salt that deposits on the wood surface increases to a level that can be observed. Note that salt accumulation is not an issue for ambient solar irradiation (1 sun) since the relatively slow evaporation rates at lower illumination intensities hinder the salt's ability to reach its crystallization concentration. Nevertheless, the salt that accumulates after 10 h of operation under 5 suns does not noticeably reduce the steam generation performance. Furthermore, the bilayer wood exhibits a unique self-regenerating ability, where the precipitated salt within the wood structure rapidly dissolves (for water soluble salts such as NaCl and KCl) and/or falls (for sparingly soluble salts such as calcium carbonate, calcium sulfate, and magnesium hydroxide) back to the surrounding seawater at night (Figure S17, Supporting

Information). The evaporation performance under different solar concentration cycles is shown in Figure 5B. After 25 cycles under various illumination intensities, the water extraction rate remains the same as the first cycle under 1 sun. This demonstrates the stability and self-regenerating ability of the bilayer wood water desalination device. The salt accumulation–dissolution self-regenerating process is believed to originate from the unique microstructures within the bilayer wood, including: (1) the through-channel connection between the light absorption layer (carbonized layer) and the liquid guiding layer (original vascular wood structure) as well as (2) the large dimensions of the wood channel (lumen) structures (on the order of tens of microns) that ensure efficient mass exchange and promote rapid dissolution of the accumulated salt.

Beyond stable performance, cost and scalability are essential for practical applications. The only material used to create the proposed device is basswood, which is a renewable and readily available material in nature. To create the proposed water extraction material, a single-step surface carbonization process was employed. Therefore, the material and processing cost is exceptionally low, which makes the bilayer wood a cost-effective water extraction material. The estimated price is below \$1 m⁻² based on the raw materials, which is much lower than any other reported solar steam material to date (≈\$6 m⁻²).^[1] Note that assembling bilayer wood blocks into a large panel is readily achievable and of importance for industrial applications (Figure 5C; Figure S18, Supporting Information). To demonstrate scalability, we assembled a large bilayer wood panel (22 cm × 18 cm) using 20 pieces

of smaller bilayer wood blocks (4.4 cm × 4.5 cm). The desalination effects of the bilayer wood were systematically evaluated using different water samples, including water (with different ions) from the Dead Sea and the Chesapeake Bay. The most common ions present in both seawater and groundwater were employed to demonstrate the concept of water purification. Specifically, the concentrations of Na⁺, Mg²⁺, K⁺, and Ca²⁺ ions after desalination are 3.98, 0.24, 0.32, and 12.70 mg L⁻¹ for the Chesapeake Bay and 3.60, 0.52, 0.82, and 29.0 mg L⁻¹ for the Dead Sea, respectively, as determined using inductively coupled plasma mass spectrometry (ICP-MS). (Figure 5D). These ion concentrations are much lower compared to the initial seawater used for the clean water extraction process. The reason that small amounts of ions can be detected in the evaporated water could be due to trace amounts of seawater in the evaporated steam. Note that the reported ion concentration values meet the World Health Organization (WHO) and the US Environmental Protection Agency (EPA) standards.^[36] It should also be noted that heavy metals and biological toxins are also present in seawater. However, since neither heavy metals nor biological toxins can evaporate along with the steam, we anticipate that the concentration of these toxic species would be within an acceptable range if the water vapor was retrieved.

For the first time, we demonstrated a tree-inspired design as a high-performance solar energy harvester and steam generator with additional capabilities: water desalination and groundwater extraction from sand/soil. The reported tree-inspired design is a unique bilayer structure derived from natural basswood with a carbonized top surface. The carbonized wood surface retains the natural, hierarchical wood mesostructure (vessels, fiber tracheids, and lumen) and acts as a light absorption layer capable of harvesting 99% of the incident light due to 3D absorption effects. The natural basswood, possessing aligned channels composed of hydrophilic cellulose microfibrils, can effectively pump water vertically. The bilayer wood enables water extraction when inserted into a range of media, including sand, soil, and seawater, using a solar steam mechanism. The device also demonstrates long-term stability in seawater without salt accumulation. Groundwater extraction (directly from sand and soil) is also feasible with the unique bilayer wood device with an evaporation rate as high as 11 kg m⁻² h⁻¹. In terms of water extraction from seawater, the reported ion concentration values meet the WHO and the US EPA standards. The exceptional water extraction performance is due to the unique optical, thermal, and fluidic properties of the bilayer wood. Future optimization of the all-wood device can be foreseen using other types of wood and tailored microstructures. The naturally abundant and low-cost bilayer wood (≈\$1 m⁻², much lower than any other existing technologies) offers a practical solar energy conversion and water extraction solution (from seawater, sand, and soil) capable of providing large-scale clean water to remote, arid, or disaster-relief areas. The reported inexpensive and efficient tree-inspired all-wood design addresses the main material challenges that typically prohibit the large-scale application of solar energy harvesters and steam generators.

Experimental Section

Fabrication Process of Bilayer Wood for Solar-Driven Water Desalination: A wood log was cut perpendicular to the wood growth direction to form

wood blocks (4.4 cm × 4.5 cm). The blocks were then pressed on a hot plate at 500 °C to carbonize the top surface. The thickness of the carbon layer was controlled based on the carbonization time. For example, the conventional carbonization time (30 s) created a layer ≈3 mm thick. After carbonization, the top surface of the carbon layer was carefully polished with 2000 grit sandpaper and the residual carbon was removed with compressed air.

Optical Measurements: The absorption spectrum was measured by an UV-vis Spectrometer Lambda 35 from 250–2500 nm (PerkinElmer, USA). An integrating sphere was used to collect the reflected light. Note that multiple samples of bilayer wood, amorphous carbon, and natural wood were tested.

Water Extraction from Sand, Soil and Seawater: All of the solar desalination experiments were conducted using a custom optical measurement system, which includes a multifunctional solar simulator (Newport Oriel 69907) as well as optical components (Newport Oriel 67005). The optical intensity on the top wood surface could be easily adjusted by controlling the power of the solar simulator and the distance of the optical lens. The Thorlabs PM100D power meter precisely recorded the optical intensity on the wood sample. The partially carbonized wood blocks were placed in a glass chamber filled with seawater and sand. Note that the salt concentrations of the seawater and groundwater used in this work were the same (≈3 wt%). To accurately measure the evaporation rates, the illuminated wood samples were put on a properly calibrated electronic balance (Citizen CX301, accuracy: 0.1 mg) and were recorded in real-time with a digital video camera. The irradiated area on the wood sample was ≈3.24 cm². Simultaneously, the temperature of the bulk seawater, soil, and sand as well as the carbonized top wood layer was measured with two thermometers (Omega HH74K).

Thermal Conductivity Measurement: The inplane thermal conductivity measurement was based on steady state Fourier's heat conduction theory. The samples were cut into small pieces (6 mm width, 30 mm length, and 1 mm thickness) that fit within the test fixture. Calibration experiments were performed on pure glass ($k = 1 \text{ W m}^{-1} \text{ K}^{-1}$) and stainless steel ($16 \text{ W m}^{-1} \text{ K}^{-1}$) before testing the wood samples to ensure the accuracy of measurements.

IR Measurements: A FLIR Merlin MID IR camera was used to characterize the sample's thermal properties under different test conditions. The solar simulator was employed as the heat source that illuminated the top of the wood samples at various intensities: 1–10 suns. The wood's temperature distribution was monitored and recorded with the IR camera. The high-resolution IR camera (320 × 256 pixels) detected the IR radiation in a specified wavelength range (1–5.4 μm) and the ThermCAM Research software interpreted the temperature distribution of the wood samples.

Supporting Information

Supporting information is available from the Wiley Online Library or from the author.

Acknowledgements

The authors acknowledge the support of the Maryland Nanocenter, its Surface Analysis Center, and AIMLab. M.Z. and Y.L. acknowledge the financial support by the Jiangsu Provincial Department of Education (JPDE) and China Scholarship Council (CSC), respectively. S.D.L. acknowledges the support by the Department of Defense (DoD) through the National Defense Science and Engineering Graduate (NDSEG) Fellowship Program.

Conflict of Interest

The authors declare no conflict of interest.

Keywords

high efficiency, light trapping, solar energy harvesting, solar steam generation, tree-inspired design

Received: July 22, 2017
Revised: September 3, 2017
Published online:

-
- [1] G. Ni, G. Li, S. V. Borisikina, H. Li, W. Yang, T. Zhang, G. Chen, *Nat. Energy* **2016**, *1*, 16126.
- [2] D. Kraemer, B. Poudel, H.-P. Feng, J. C. Caylor, B. Yu, X. Yan, Y. Ma, X. Wang, D. Wang, A. Muto, K. McEnaney, M. Chiesa, Z. Ren, G. Chen, *Nat. Mater.* **2011**, *10*, 532.
- [3] L. Zhou, Y. Tan, J. Wang, W. Xu, Y. Yuan, W. Cai, S. Zhu, J. Zhu, *Nat. Photonics* **2016**, *10*, 393.
- [4] L. Zhou, Y. Tan, D. Ji, B. Zhu, P. Zhang, J. Xu, Q. Gan, Z. Yu, J. Zhu, *Sci. Adv.* **2016**, *2*, e1501227.
- [5] S. P. Surwade, S. N. Smirnov, I. V. Vlassiuk, R. R. Unocic, G. M. Veith, S. Dai, S. M. Mahurin, *Nat. Nanotechnol.* **2015**, *10*, 459.
- [6] H. Ghasemi, G. Ni, A. M. Marconnet, J. Loomis, S. Yerci, N. Miljkovic, G. Chen, *Nat. Commun.* **2014**, *5*, 4449.
- [7] Y. Ito, Y. Tanabe, J. Han, T. Fujita, K. Tanigaki, M. Chen, *Adv. Mater.* **2015**, *27*, 4302.
- [8] Q. Jiang, L. Tian, K.-K. Liu, S. Tadepalli, R. Raliya, P. Biswas, R. R. Naik, S. Singamaneni, *Adv. Mater.* **2016**, *28*, 9400.
- [9] Y. Liu, S. Yu, R. Feng, A. Bernard, Y. Liu, Y. Zhang, H. Duan, W. Shang, P. Tao, C. Song, T. Deng, *Adv. Mater.* **2015**, *27*, 2768.
- [10] O. Neumann, A. S. Urban, J. Day, S. Lal, P. Nordlander, N. J. Halas, *ACS Nano* **2013**, *7*, 42.
- [11] K. Bae, G. Kang, S. K. Cho, W. Park, K. Kim, W. J. Padilla, *Nat. Commun.* **2015**, *6*, 10103.
- [12] G. Xue, K. Liu, Q. Chen, P. Yang, J. Li, T. Ding, J. Duan, B. Qi, J. Zhou, *ACS Appl. Mater. Interfaces* **2017**, *9*, 15052.
- [13] N. Xu, X. Hu, W. Xu, X. Li, L. Zhou, S. Zhu, J. Zhu, *Adv. Mater.* **2017**, *29*, 1606762.
- [14] X. Hu, W. Xu, L. Zhou, Y. Tan, Y. Wang, S. Zhu, J. Zhu, *Adv. Mater.* **2017**, *29*, 1604031.
- [15] K. K. Liu, Q. Jiang, S. Tadepalli, R. Raliya, P. Biswas, R. R. Naik, S. Singamaneni, *ACS Appl. Mater. Interfaces* **2017**, *9*, 7675.
- [16] X. Li, W. Xu, M. Tang, L. Zhou, B. Zhu, S. Zhu, J. Zhu, *Proc. Natl. Acad. Sci. USA* **2016**, *113*, 13953.
- [17] H. M. Qiblawey, F. Banat, *Desalination* **2008**, *220*, 633.
- [18] D. C. DiGiulio, R. B. Jackson, *Environ. Sci. Technol.* **2016**, *50*, 4524.
- [19] P. Beaumont, *Ground Water* **1973**, *11*, 23.
- [20] F. Nestmann, P. Oberle, M. Ikhwan, D. Stoffel, *Procedia Eng.* **2013**, *54*, 58.
- [21] H. Zhu, W. Luo, P. N. Ciesielski, Z. Fang, J. Y. Zhu, G. Henriksson, M. E. Himmel, L. Hu, *Chem. Rev.* **2016**, *116*, 9305.
- [22] V. Volkov, A. H. De Boer, *Plant, Cell Environ.* **2003**, *2003*, 87.
- [23] U. Zimmermann, H. Schneider, L. H. Wegner, A. Haase, *New Phytol.* **2004**, *162*, 575.
- [24] Y. H. Jung, T.-H. Chang, H. Zhang, C. Yao, Q. Zheng, V. W. Yang, H. Mi, M. Kim, S. J. Cho, D.-W. Park, H. Jiang, J. Lee, Y. Qiu, W. Zhou, Z. Cai, S. Gong, Z. Ma, *Nat. Commun.* **2015**, *6*, 7170.
- [25] Q. Wang, J. Y. Zhu, J. M. Considine, *ACS Appl. Mater. Interfaces* **2013**, *5*, 2527.
- [26] K. M. O. Håkansson, A. B. Fall, F. Lundell, S. Yu, C. Krywka, S. V Roth, G. Santoro, M. Kvick, L. Prahl Wittberg, L. Wägberg, L. D. Söderberg, *Nat. Commun.* **2014**, *5*, 4018.
- [27] M. Hamed, E. Karabulut, A. Marais, A. Herland, G. Nyström, *Angew. Chem., Int. Ed.* **2013**, *52*, 12038.
- [28] M. J. Lundahl, A. G. Cunha, E. Rojo, A. C. Papageorgiou, L. Rautkari, J. C. Arboleda, O. J. Rojas, *Sci. Rep.* **2016**, *6*, 30695.
- [29] M. S. Toivonen, A. Kaskela, O. J. Rojas, E. I. Kauppinen, O. Ikkala, *Adv. Funct. Mater.* **2015**, *25*, 6618.
- [30] J. S. Sperry, *Int. J. Plant Sci.* **2003**, *164*, S115.
- [31] A. Nardini, S. Salleo, S. Jansen, *J. Exp. Bot.* **2011**, *62*, 4701.
- [32] G. Compagnini, *Appl. Opt.* **1994**, *33*, 7377.
- [33] S. Das, S. K. Mitra, *Phys. Rev. E: Stat., Nonlinear, Soft Matter Phys.* **2013**, *87*, 1.
- [34] D. Quéré, *Europhys. Lett.* **1997**, *39*, 533.
- [35] H. Mehrabian, J. J. Feng, *J. Fluid Mech.* **2014**, *752*, 670.
- [36] Safe Drinking-water from Desalination (WHO, 2011), http://www.who.int/water_sanitation_health/publications/desalination_guidance/en/, (accessed: June 2016).